DC Voltage and Torque Ripple Mitigation in Modular PMSG Drives for Off-Shore Multi-MW WECSs with Linear SPWM modulation

K. ElShawarby, A. Di Gerlando, G. M. Foglia, R. Perini
POLITECNICO DI MILANO
Via La Masa 34
20156 Milano, Italy
Phone: +39 (02) 23993722
Email: {khaled.elshawarby, antonino.digerlando, gianmaria.foglia, roberto.perini}@polimi.it

Keywords

≪Off-shore Wind turbines≫, ≪Sequential Command≫, ≪Series connected≫, ≪Multi-modular machines≫, ≪Harmonic elimination≫

Abstract

A multi-modular axial flux machine is used for wind energy conversion systems (WECSs) where each module is connected to its own two-level converter. All converters are connected in series at the DC side to allow HVDC transmission. In the paper, an in-depth reasoning for the control of each individual voltage. A phase shift between PWM carrier signals of the neighbouring converters is implemented. A mathematical analysis is carried out. A criterion for the best choice of the phase shift to minimize dc voltage and torque harmonics is proposed.

Introduction

In recent years, with the development in renewable energy systems, projects using transmission and distribution grid are more and more applied [1, 2]. Advancements in power electronics are making High Voltage Direct Current (HVDC) transmission systems more reliable. HVDC is considered an economic solution for energy transmission since it allows power transport over long distances with low losses [3, 4].

Axial-flux permanent-magnet (AFPM) machines have been under keen research interest in the last decade as an alternative to conventional radial-flux PM machines, particularly for low-speed direct-drive applications (e.g. wind generators), due to their advantages of flexible disk shape, compact and rugged construction, adjustable flat (plane) airgap, high power density and high torque-to-weight ratio [5]. A multi-modular (MM) AFPM synchronous generator (SG) allows the machine to reach high generation power with the same radial length. Moreover, the MM configuration allows for a redundant operation: in case of fault in one of the modules, operation can continue with decreased output power.

This paper presents a MM AFPMSG directly driven (DD) by an off-shore wind turbine. Each machine module is connected to a two-level IGBT converter where all converters are connected in series on the DC side. As the number of modules increases, the voltage across the DC bus increases which allows to reach the usual levels for HVDC transmission. A shift between the carrier signals of parallel converters is introduced in order to cancel targeted harmonics: such a concept is called Sequential Command [7, 8]. However, in this paper Sequential Command SPWM is used for the converters connected in series along with the illustration of the control techniques for the converters. The aim is the mitigation of ripples in torque and DC voltage and it is achieved by a coordinated control of the converters.

Moreover, the high degree of modularity (both for the electromechanical actuator and for the electronic converter) allows the use of two-level standard converters based on a very mature technology and the

reduction of voltage and current ratings of each module. This makes it possible to use standard off-the-shelf power electronics and a more effective reliability and redundancy, thanks to the absence of magnetic mutual coupling between AFPMSG modules.

The paper is divided as follows: Section II presents the off-shore WECSs along with the rated data of each module of AFPMSG. Section III deals with the machine control for various converters connected in series, highlighting the necessity of the voltage control of each converter. Section IV derives the expression of the DC bus voltage presenting the harmonics of the DC bus voltage and electromagnetic torque amplitudes for the overall speed range of the machine from the cut-in speed up to the rated speed. Finally, in Section V, the simulation results are presented for four different cases: one module AFPMSG and sequential command applied for two, three and four modules AFPMSG. A comparison between the theoretical analysis and simulation results is done highlighting the high accuracy of the derived expressions.

Proposed system for Off-shore WECSs

The WECS under study is represented in Figure 1 where all the rotors of the MM AFPMSG are fastened on the same shaft and aligned with one another. Each module is connected to a 2 kV two-level IGBT AC-DC converter and all converters are connected in series at the DC side. $v_{dc\mu}$ is the DC bus voltage of each converter module μ and the total voltage across the DC bus is v_{dc_T}.

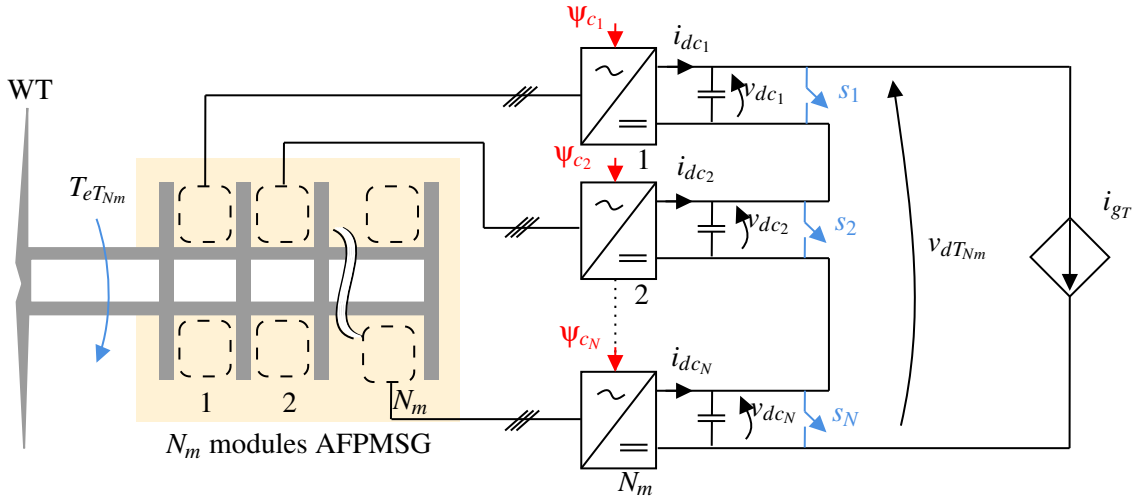

Fig. 1: Schematic of the modular direct-drive axial-flux PMSG under study. Each module of the machine is connected to a two-level converter. All the two-level converters are connected in series at the DC side.

Table I: single module axial flux permanent magnet machine nameplate data

P_n [MW], I_n [A]	1.0 , 713
Rated frequency f_{rated} [Hz], N. of poles p	14.73, 104
Rated Speed Ω_n [rpm]	17
Line to neutral EMF at rated speed [V] (sinusoidal waveform)	435
Phase resistance R_s [mΩ]	14.59
Synchronous inductance (d,q axes) L_s [mH]	4.321
Rotor ext. diameter [m], Axial length [m]	5.00, 0.603
No damping cage	

To ensure continuity in case of fault occurrence, switch s_μ is closed in case of fault in module μ and generation continues at reduced output. The AFPMSG was designed according to the procedure illustrated in [6] and the assumed rated data for each module μ are reported in Table I. Since the machine is isotropic, the d- and q-axis inductances are equal. The carrier signals of the neighbouring converters achieve the

shift between the harmonic components of the voltage and torque without affecting the DC components for both quantities. The grid-side converter which is modelled as a current controlled source i_{gT}

Series Converters DC bus voltage control

A series configuration of the converters can be adopted in order to increase the voltage level of the output for HVDC transmission. However, unlike the parallel connected converter case, a voltage control must be implemented to each converter connected in series, otherwise the system becomes unstable.

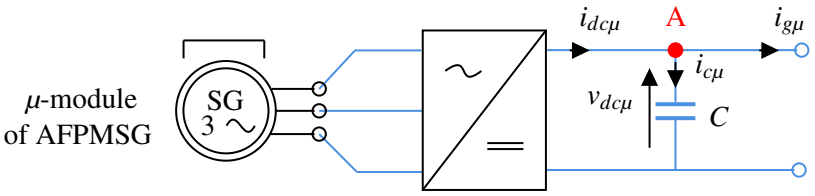

Fig. 2: Equivalent circuit of μ module of AFPMSG connected to a generic converter

Starting from the voltage equations of a generic module μ of the AFPMSG (fig. 2) in dq reference frame and from KCL at node A:

$$\begin{aligned} v_{sd\mu} &= R_s i_{sd\mu} + L_s p i_{sd\mu} - \omega_m L_s i_{sq\mu} \\ v_{sq\mu} &= R_s i_{sq\mu} + L_s p i_{sq\mu} + \omega_m L_s i_{sd\mu} + \omega_m \psi_{PM} \\ i_{dc\mu} &= C p v_{dc\mu} + i_{g\mu} \end{aligned} \tag{1}$$

where ω_m is the angular frequency of the machine, ψ_{PM} is the stator flux linkage due to PM, R_s, L_s are the resistance and synchronous inductance respectively. Finally p is derivative operator with respect to time t. Applying the power balance across the converter assuming a lossless converter $\left(v_{dc\mu} i_{dc\mu} = v_{sd\mu} i_{sd\mu} + v_{sq\mu} i_{sq\mu}\right)$ and multiplying the equations of (1) by $i_{sd\mu}$ and $i_{sq\mu}$ respectively, (1) becomes:

$$\begin{cases} v_{sd\mu} i_{sd\mu} = \left(R_s + \dfrac{L_s}{2} p\right) i_{sd\mu}^2 - \omega_m L_s i_{sq\mu} i_{sd\mu} \\ v_{sq\mu} i_{sq\mu} = \left(R_s + \dfrac{L_s}{2} p\right) i_{sq\mu}^2 + \omega_m L_s i_{sd\mu} i_{sq\mu} + \omega_m \psi_{PM} i_{sq\mu} \end{cases} \tag{2}$$

Summing the equations in (2) gives the AC power produced by the PMSG and the coupling terms are cancelled. The equation becomes:

$$\begin{aligned} v_{sd\mu} i_{sd\mu} + v_{sq\mu} i_{sq\mu} &= \left(R_s + \frac{L_s}{2} p\right)\left(i_{sd\mu}^2 + i_{sq\mu}^2\right) + \omega_m \psi_{PM} i_{sq\mu} \\ v_{sd\mu} i_{sd\mu} + v_{sq\mu} i_{sq\mu} &= v_{dc\mu}\left(C p v_{d_\mu} + i_{g\mu}\right) \end{aligned} \tag{3}$$

The small signal analysis is applied to (3), adopting $i_{g\mu} = I_{g\mu}$; $v_{dc\mu} = V_{dc\mu} + \Delta v_{dc\mu}$; $i_{sd\mu} = I_{sd\mu} + \Delta i_{sd\mu}$; $i_{sq\mu} = I_{sq\mu} + \Delta i_{sq\mu}$. By assuming $I_{sd\mu} = 0$ to ensure maximum machine torque and $(\Delta i_{sd\mu}^2, \Delta i_{sd\mu}^2, \Delta v_{dc\mu}^2) \simeq 0$, (3) yields to:

$$V_{dc\mu} C p\left(\Delta v_{dc\mu}\right) + V_{dc\mu} I_{g\mu} + \Delta v_{dc\mu} I_{g\mu} = R_s I_{sq\mu}^2 + 2\left(R_s + \frac{L_s}{2} p\right) I_{sq\mu} \Delta i_{sq\mu} + \omega_m \psi_{PM} I_{sq\mu} + \omega_m \psi_{PM} \Delta i_{sq\mu}$$

(4)

where, (4) represents two contributions: a steady state and a variating component. The logic behind a controller design is to eliminate variation (i.e. error (ε)=0). Thus, focusing on the variating component and equating the expression to zero, (4) becomes:

$$\begin{cases} V_{dc\mu} I_{g\mu} = R_s I_{sq\mu}^2 + \omega_m \psi_{PM} I_{sq\mu} \\ \left(V_{dc\mu} Cp + I_{g\mu}\right) \Delta v_{dc\mu} - \left(\left(2R_s + L_s p\right) I_{sq\mu} + \omega_m \psi_{PM}\right) \Delta i_{sq\mu} = 0 \end{cases} \tag{5}$$

Equation (5b) shows a generic disturbance to be compensated in a generic AFPMSG μ-module where two disturbances exist: dc bus voltage disturbance $\Delta v_{dc\mu}$ and q axis current disturbance $\Delta i_{sq\mu}$. Two cases will be studied: the parallel and series configurations in order to identify the differences among them. For sake of simplicity, a two-module AFPMSG connected to two converters is considered ($\mu = 1,\ 2$) as shown in figure 3.

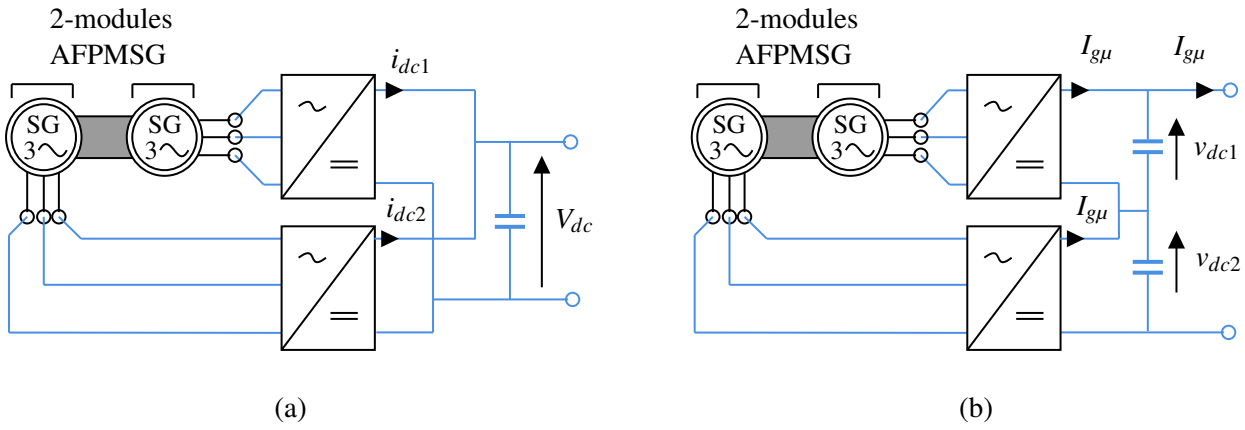

Fig. 3: Equivalent circuit of two-module AFPMSG (a) parallel connection to the converters (b) series connection of the converters

Parallel connection

For the parallel connection, both the DC bus voltage and its disturbance for both converters is the same. Thus, substituting in (5b) for $(\mu = 1,2)$ and $\Delta v_{dc1} = \Delta v_{dc2} = \Delta v_{dc}$, the expression can be written as:

$$\frac{\left(\left(2R_s + L_s p\right) I_{sq1} + \omega_m \psi_{PM}\right)}{\left(V_{dc} Cp + I_{g1}\right)} \Delta i_{sq1} - \frac{\left(\left(2R_s + L_s p\right) I_{sq2} + \omega_m \psi_{PM}\right)}{\left(V_{dc} Cp + I_{g2}\right)} \Delta i_{sq2} = 0 \tag{6}$$

Since the two modules of the machine are identical, the steady state quantities of q current for both modules are the same ($I_{sq1} = I_{sq2} = I_{sq}$). Moreover, the grid contribution of each converters is the same as well ($I_{g1} = I_{g2} = I_g$). Therefore, equation (6) can be simplified into:

$$\frac{\left(\left(2R_s + L_s p\right) I_{sq} + \omega_m \psi_{PM}\right)}{\left(V_{dc} Cp + I_g\right)} \left(\Delta i_{sq1} - \Delta i_{sq2}\right) = 0 \tag{7}$$

As highlighted in equation (7), the only quantities to be controlled are the variations across q axes currents of different machine modules. Thus, no additional voltage controllers are to be added for the control of the machine and the classic vector control is sufficient for the correct operation of the machine.

Series connection

As for the series connection, the current contribution to the grid of each converter is the same. Thus, substituting in (5b) for $(\mu = 1,2)$ and $I_{g1} = I_{g2} = I_g$, the expression can be written as:

$$\begin{aligned}\Big((2R_s + L_s p)I_{sq1} + \omega_m \psi_{PM}\Big)\frac{\Delta i_{sq1}}{\Delta v_{dc1}} - V_{dc1}C\frac{p(\Delta v_{dc1})}{\Delta v_{d1c}} \\ = \Big((2R_s + L_s p)I_{sq2} + \omega_m \psi_{PM}\Big)\frac{\Delta i_{sq2}}{\Delta v_{dc2}} - V_{dc2}C\frac{p(\Delta v_{dc2})}{\Delta v_{dc2}}\end{aligned} \tag{8}$$

Again, since the modules are identical ($I_{sq1} = I_{sq2} = I_{sq}$) and the DC bus voltage sharing should be the same ($V_{dc1} = V_{dc2} = V_{dc}$), equation (8) can be simplified into:

$$\Big((2R_s + L_s p)I_{sq} + \omega_m \psi_{PM}\Big)\left(\frac{\Delta i_{sq1}}{\Delta v_{dc1}} - \frac{\Delta i_{sq2}}{\Delta v_{dc2}}\right) + V_{dc}C\left(\frac{p\Delta v_{dc2}}{\Delta v_{dc2}} - \frac{p\Delta v_{dc1}}{\Delta v_{dc1}}\right) = 0 \tag{9}$$

Comparing equations (9) and (7), the difference between the parallel and series converters configurations is highlighted such that the disturbance across the DC bus voltage $\Delta v_{dc\mu}$ has to be controlled.

Since $I_{sd\mu}$ has to be kept to zero for achieving maximum torque produced by the machine, the DC bus voltage has to be controlled as well by the q axis current control. Thus a second contribution to the q axis current reference $i_{sq}^{ref,b}$ has to be included in the control loop as shown in figure 4.

In order to avoid a stiff control, $(N_m - 1)$ DC voltage controllers are implemented. In this way the uncontrolled converter voltage will remain floating in order to compensate for any disturbances or change of system state that may occur. The cut-off frequency of the voltage control loop has to be at least ten times slower than that of the current controller.

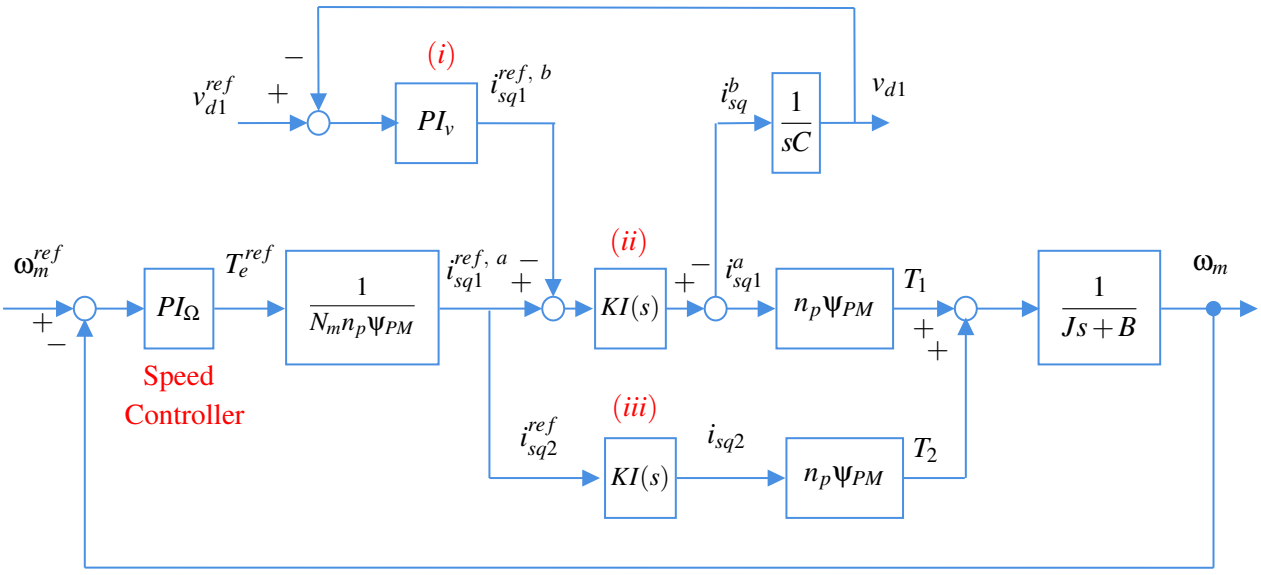

Fig. 4: Modified q axis control scheme for two modules AFPMSG series converters including the control loop of the DC bus voltage for the first converter where (i) is the voltage PI controller, (ii) is the current closed loop for the first converter and (iii) is the current close loop for the second converter.

Instantaneous DC side Voltage, Electromagnetic Torque of one module

An approximate mathematical expression for the dc side current $i_{dc\mu}$ for each converter under SPWM conditions was provided in [8]. Assuming that all the ripple components in $i_{dc\mu}$ flow in the capacitor of each module, an approximate expression for the dc bus capacitor voltage of each module μ under SPWM modulation can be derived as the integration of the $i_{dc\mu}$ ripple components divided by the value of the capacitance C. Thus:

$$
\begin{aligned}
v_{d\mu}(t) = \frac{3}{2V_d \cdot \omega \cdot C} \Bigg[& \frac{V_1 I_{m_f-2}}{(m_f-3)} \cos\Big((m_f-3)\,\omega t + \psi_{c_\mu} - \theta_{m_f-2}\Big) + \frac{V_{m_f-2} I_1}{(m_f-3)} \cos\big((m_f-3)\,\omega t + \psi_{c_\mu} + \phi\big) \\
& + \frac{V_{m_f+2} I_{2m_f-1}}{(m_f-3)} \cos\Big((m_f-3)\,\omega t + \psi_{c_\mu} - \theta_{2m_f-1}\Big) + \frac{V_{2m_f-1} I_{m_f+2}}{(m_f-3)} \cos\Big((m_f-3)\,\omega t + \psi_{c_\mu} + \theta_{m_f+2}\Big) \\
& + \frac{V_1 I_{mf+2}}{(m_f+3)} \cos\big((m_f+3)\,\omega t + \psi_{c_\mu} - \theta_{mf+2}\big) + \frac{V_{mf-2} I_{2mf+1}}{(m_f+3)} \cos\big((m_f+3)\,\omega t + \psi_{c_\mu} - \theta_{2mf+1}\big) \\
& + \frac{V_{m_f+2} I_1}{(m_f+3)} \cos\big((m_f+3)\,\omega t + \psi_{c_\mu} - \phi\big) + \frac{V_{2m_f+1} I_{m_f-2}}{(m_f+3)} \cos\Big((m_f+3)\,\omega t + \psi_{c_\mu} + \theta_{m_f-2}\Big) \\
& + \frac{V_1 I_{2m_f-1}}{(2m_f)} \cos\Big((2m_f)\,\omega t + 2\psi_{c_\mu} - \theta_{2m_f-1}\Big) + \frac{V_1 I_{2m_f+1}}{(2m_f)} \cos\Big((2m_f)\,\omega t + 2\psi_{c_\mu} - \theta_{2m_f+1}\Big) \\
& + \frac{V_{m_f-2} I_{m_f+2}}{(2m_f)} \cos\Big((2m_f)\,\omega t + 2\psi_{c_\mu} - \theta_{m_f+2}\Big) + \frac{V_{m_f+2} I_{m_f-2}}{(2m_f)} \cos\Big((2m_f)\,\omega t + 2\psi_{c_\mu} - \theta_{m_f-2}\Big) \\
& + \frac{V_{2m_f-1} I_1}{(2m_f)} \cos\big((2m_f)\,\omega t + 2\psi_{c_\mu} - \phi\big) + \frac{V_{2m_f+1} I_1}{(2m_f)} \cos\big((2m_f)\,\omega t + 2\psi_{c_\mu} + \phi\big) \\
& + \frac{V_{m_f-2} I_{2m_f-1}}{(3m_f-3)} \cos\Big((3m_f-3)\,\omega t + 3\psi_{c_\mu} - \theta_{2m_f-1}\Big) + \frac{V_{2m_f-1} I_{m_f-2}}{(3m_f-3)} \cos\Big((3m_f-3)\,\omega t + 3\psi_{c_\mu} - \theta_{m_f-2}\Big) \\
& + \frac{V_{m_f+2} I_{2m_f+1}}{(3m_f+3)} \cos\Big((3m_f+3)\,\omega t + 3\psi_{c_\mu} - \theta_{2m_f+1}\Big) + \frac{V_{2m_f+1} I_{m_f+2}}{(3m_f+3)} \cos\Big((3m_f+3)\,\omega t + 3\psi_{c_\mu} - \theta_{m_f+2}\Big) \\
& + \frac{V_{2m_f-1} I_{2m_f+1}}{(4m_f)} \cos\Big((4m_f)\,\omega t + 4\psi_{c_\mu} - \theta_{2m_f+1}\Big) + \frac{V_{2m_f+1} I_{2m_f-1}}{(4m_f)} \cos\Big((4m_f)\,\omega t + 4\psi_{c_\mu} - \theta_{2m_f-1}\Big) \Bigg]
\end{aligned}
\tag{10}
$$

In (10) ϕ is the phase displacement between voltage and current fundamental components, δ the load angle, m_f the SPWM frequency modulation ratio, ω the output fundamental angular frequency, ψ_{c_μ} the phase shift applied to the carrier signal. V_{hn} are the voltage harmonic amplitudes. I_{hm} and θ_{hm} are the current harmonic amplitudes and their characteristic angles, respectively. They are obtained by applying each voltage harmonic V_{hm}, calculated in [8], to the equivalent $R-L-e$ circuit of the AFPMSG.

Table II summarizes the voltage harmonics present in (10). It should be noted that the harmonic content of the torque along with the corresponding shift in the carrier ψ_c coincides with the values in Table II [9]. Figure 5 shows the relation between the change of phase of DC voltage and torque harmonics and the change of the carrier signal phase ψ_c.

Table II: Harmonic content in the DC bus voltage ripple and electromagnetic torque. For each harmonic, the phase component due to the shift ψ_{c_μ} of the carrier signal is reported

h	**Phase component due to shift $\psi_{c}\mu$**
$m_f \pm 3$	ψ_{c_μ}
$2m_f$	$2\psi_{c_\mu}$
$3m_f \pm 3$	$3\psi_{c_\mu}$
$4m_f$	$4\psi_{c_\mu}$

In order to identify which harmonics to be cancelled via the sequential command, the derived expressions of $v_{d\mu}$ and $T_{e\mu}$ as a function of multiples of $\psi_{c\mu}$ are the key. By means of (10) and the equations derived in [9], the amplitude of any voltage or torque harmonic can be evaluated at any given speed. The amplitudes of the main harmonics for both voltage and torque reported in Table II are shown in Fig. 6, as a function of the machine speed expressed as the frequency of the PWM control signals. The chosen frequency ratio m_f is as low as 15 in order to limit the switching losses. The power generation to the grid starts from the cut-in speed (normally 0.3-0.35·Ω_n) up to the rated one Ω_n.

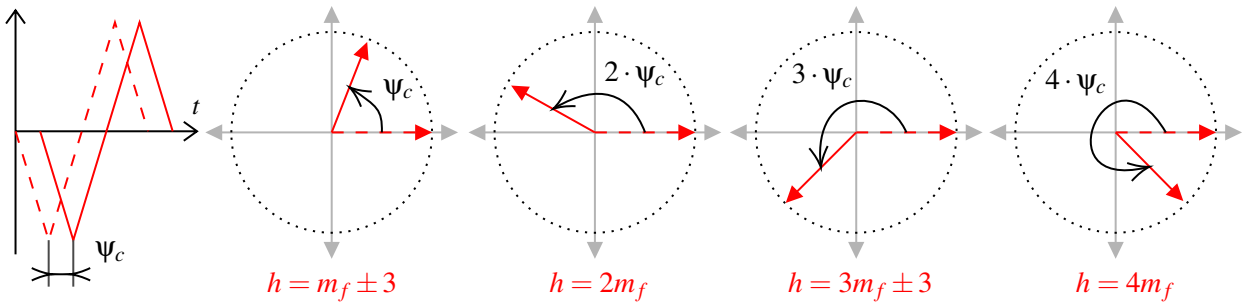

Fig. 5: The relation between the change of the carrier signal phase ψ_c and its effect on the phase of the harmonics of DC voltage and torque reported in Table II.

A common approach for the choice of the harmonic to eliminate is the least order harmonic ($m_f - 3$). However, in a single module, the most dominant harmonic in both the DC voltage and electromagnetic torque for the frequency range of the machine is the harmonic of the order $2m_f$ as shown in fig. 6. In fact, two converter modules connected in series with a shift of 90^o provide a much lower THD% for both overall voltage and torque than with a shift of 180^o (Fig. 7a) all along the frequency range. This result is verified by the much reduced peak to peak with a shift of 90^o for both the total voltage and total torque than 180^o (Fig. 7b). Despite the fact that by adopting 180^o shift, not only the harmonic $m_f - 3$ is cancelled but also the $m_f + 3$ and $3m_f \pm 3$ harmonics while the 90^o shift only provides the cancellation of $2m_f$.

Thus, for varying frequency applications (i.e. WECSs), the better shift to adopt among two parallel connected converters would be 90^o which have an overall lower THD% than 180^o.

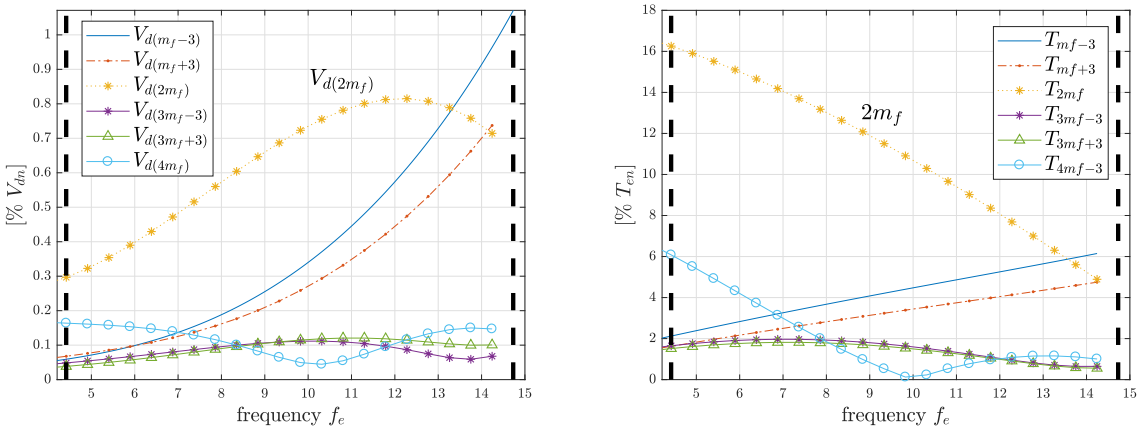

(a) (b)

Fig. 6: Harmonic amplitudes for both voltage and torque in a single module [in %] under SPWM modulation over the speed range of the AFPMSG for $m_f = 15$.

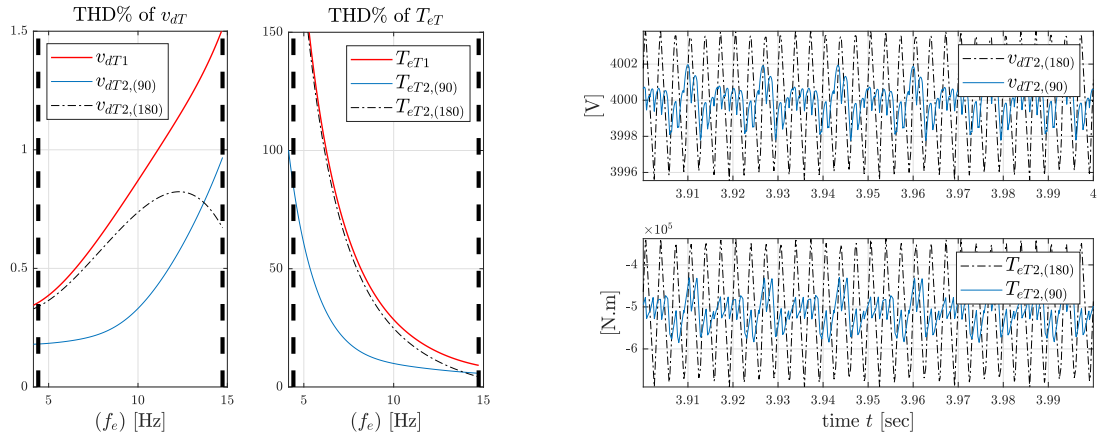

Fig. 7: A comparison between the THD% reduction when the sequential command is applied at $\psi_{c2} = 90^o$ or $\psi_{c2} = 180^o$ for the overall dc bus voltage and torque. (a) THD% of both dc bus voltage and torque (b) voltage v_{d2} and torque waveforms for a period working at a fundamental voltage of 10Hz. A much lower peak to peak for the case of 90^o compared to 180^o is apparent.

Simulation results

The system presented in Section II is implemented in Matlab/Simulink for four different cases: single module AFPMSG, two modules AFPMSG whose carriers are shifted by 90^o, three modules AFPMSG whose carriers shifted by 120^o and 240^o and four modules AFPMSG whose carriers are shifted by 90^o, 180^o and 270^o. For three and four modules, the shift angles are are selected on the basis of eliminating the least order harmonic $m_f - 3$ and also $2m_f$.

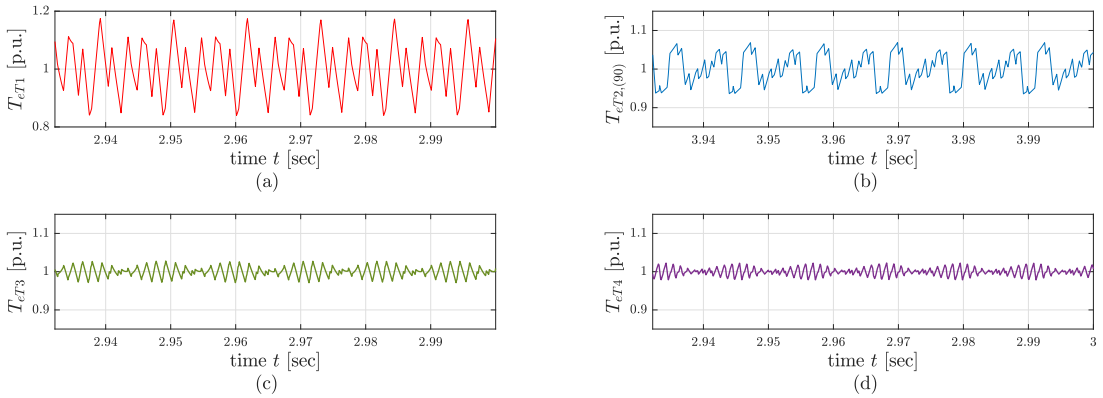

Fig. 8: Simulation waveforms of the four cases: (a) T_{eT1}, (b) $T_{eT2,(90)}$, (c) T_{eT3} and (d) T_{eT4} at rated conditions with sequential command. The effect of sequential command in harmonic cancellation is highlighted by the reduced peak to peak values.

Each module is modelled by standard two-axis d-q model of PMSM and the classical FOC is implemented, the machine is vector-controlled to operate in maximum torque-per-ampere (MTPA) conditions. In the simulation model, the total DC bus voltage is kept constant by the grid side converter which is modelled as current controlled source. Each converter capacitor is 70 mF whose nominal value is 2000V and kept constant via $N_m - 1$ voltage controllers.

Figures 8 refers to simulation results for a period at rated conditions for different cases: single module (normal SPWM), two modules whose carriers are shifted by 90^o, three modules whose carriers are shifted by 120^o, 240^o and finally a four modules whose carriers are shifted by 90^o, 180^o, 270^o. Figure 9a concerns a four-module AFPMSG, and highlights the aspect of shifted harmonics in the individual DC

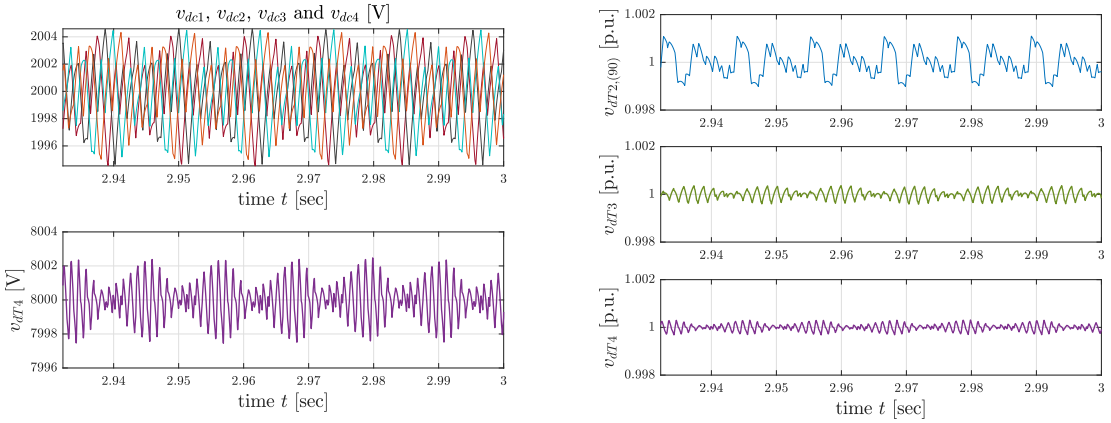

(a) (b)

Fig. 9: (a) Four-module AFPMSG DC voltages of each converters shifted by the sequential command along with the equivalent total voltage in volts (b) Simulation waveforms of $v_{dT2,(90)}$, v_{dT3} and v_{dT4} at rated conditions with sequential command in p.u.

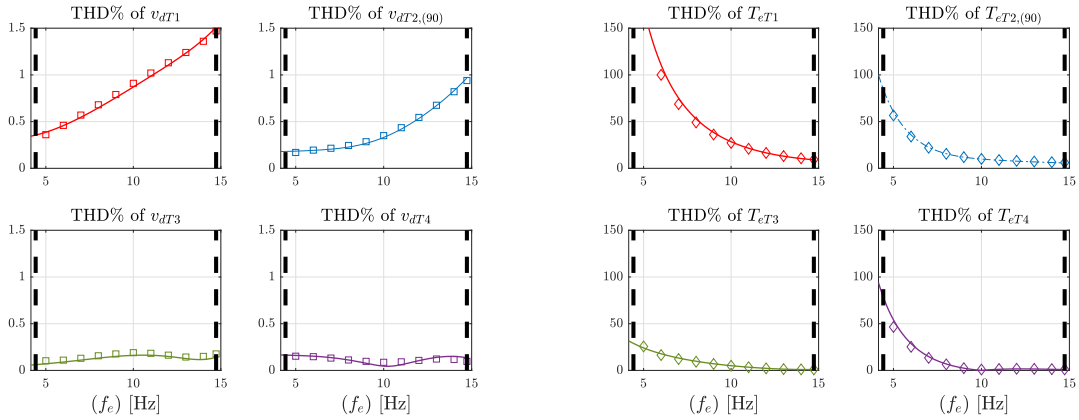

(a) (b)

Fig. 10: THD for both voltage and torque under SPWM modulation over the speed range of the AFPMSG for both theoretical and simulation results. a) DC bus voltage THD% of the four cases: THD% v_{dT1}, $v_{dT2,(90)}$, v_{dT3} and v_{dT4}. b) Electromagnetic torque THD% of the four cases: THD% T_{eT1}, $T_{eT2,(90)}$, T_{eT3} and T_{eT4}.

voltages along with the total voltage v_{d4}. Both figures emphasize that, by increasing the number of modules, the ripple content around the steady state torque decreases.

Figure 10 highlights the effect of sequential command on the THD% of v_{dT} and T_{eT} for the four different cases mentioned earlier obtained both by Matlab/Simulink and by the analytical model presented in the previous Section. Some comments can be made:

- as the number of modules increases, a significant lower THD% is achieved with sequential command for both overall torque and dc voltage for the overall speed range;
- the simulation results for both voltage (noted as squares) and the torque (noted as diamonds) coincide with the theoretical calculation of the THD% which signifies the high accuracy of proposed analytical model.

Conclusion

The paper analyzed a technique to reduce ripples of DC voltage and torque in modular axial-flux PMSG drives for off shore wind power generation. In the considered layout, several independent machine modules are driven by a common shaft and properly aligned with one another. The module ratings allow the connection of each module to a dedicated two-level converter. The resulting multi-MW modular drive maximizes redundancy and reliability using off-the-shelf power electronics converters instead of a custom multi-level converter. The reduction of ripples is achieved by a proper phase-shift of the carrier signals of converters, operated in linear PWM modulation range. Approximated expressions for DC voltage and torque ripples have been derived and the optimal phase-shift has been identified as a function of the number of modules.

The system has been simulated by Matlab/Simulink that proved the soundness of the proposed analytical model. A scaled prototype is being prepared, and future activity will concern experimental tests.

References

[1] C. Zhuo, X. Zhang, X. Zhang and X. Yang, "Analysis, Modeling and Simulation of Multi-terminal HVDC Transmission System with Short-circuit Controllable Fault Current Limiter," 2018 IEEE International Power Electronics and Application Conference and Exposition (PEAC), Shenzhen, 2018, pp. 1-6.

[2] S. Debnath and M. Chinthavali, "Control of MMC-HVDC in low-inertia weak grids," 2017 IEEE 12th International Conference on Power Electronics and Drive Systems (PEDS), Honolulu, HI, 2017, pp. 435-441.

[3] M. Blechschmidt, C. Hahn and M. Luther, "A comprehensive approach for analytical modeling of line commutated converter based multiterminal HVDC systems," 2017 52nd International Universities Power Engineering Conference (UPEC), Heraklion, 2017, pp. 1-6.

[4] C. Guo and C. Zhao, "A new technology for HVDC start-up and operation using VSC-HVDC system," 2009 IEEE Power & Energy Society General Meeting, Calgary, AB, 2009, pp. 1-5.

[5] A. A. Pop, M. Radulescu, H. Balan and H. Kanchev, "Electromagnetic torque capabilities of axial-flux and radial-flux permanent-magnet machines," 2013 4th International Symposium on Electrical and Electronics Engineering (ISEEE), Galati, 2013, pp. 1-4.

[6] A. Di Gerlando, G. Foglia, M. F. Iacchetti, R. Perini, "Axial Flux PM Machines With Concentrated Armature Windings: Design Analysis and Test Validation of Wind Energy Generators," in IEEE Transactions on Industrial Electronics, vol. 58, no. 9, pp. 3795-3805, Sept. 2011.

[7] D. Zhang, F. Wang, R. Burgos, R. Lai and D. Boroyevich, "DC-Link Ripple Current Reduction for Paralleled Three-Phase Voltage-Source Converters With Interleaving," in IEEE Transactions on Power Electronics, vol. 26, no. 6, pp. 1741-1753, June 2011.

[8] A. Di Gerlando, K. ElShawarby, G. M. Foglia, M. F. Iacchetti and R. Perini, "DC Current and Torque Ripple Mitigation in Modular PMSG Drives for Multi-MW WECSs with Linear PWM Inverter Modulation," 2018 XIII International Conference on Electrical Machines (ICEM), Alexandroupoli, 2018, pp. 1458-1464.

[9] A. Di Gerlando, K. ElShawarby, G. M. Foglia and R. Perini, "Torsional Vibration Mitigation by Harmonic Inversion through SPWM Carrier Signal Control," 2018 XIII International Conference on Electrical Machines (ICEM), Alexandroupoli, 2018, pp. 2330-2336.